Science Advances
AAAS

advances.sciencemag.org/cgi/content/full/6/2/eaax3308/DC1

Supplementary Materials for

Extensive fires in southeastern Siberian permafrost linked to preceding Arctic Oscillation

Jin-Soo Kim, Jong-Seong Kug*, Su-Jong Jeong, Hotaek Park, Gabriela Schaepman-Strub

*Corresponding author. Email: jskug@postech.ac.kr

Published 8 January 2020, *Sci. Adv.* **6**, eaax3308 (2020)
DOI: 10.1126/sciadv.aax3308

This PDF file includes:

Table S1. Correlation matrix between burned area and aerosol optical depth at 550 nm based on MISR.

	Southeastern Siberia (100°–150°E, 45°–55°N)	Northeastern Siberia (120°–180°E, 55°–70°N)
April	0.68**	0.21
May	0.73**	0.49*

* and ** indicate significance at the 95% and 99% confidence level based on a Student's *t*-test, respectively. The Aerosol Optical Depth at 550nm is obtained from the Multi-angle Imaging SpectroRadiometer (MISR) sensor by NASA (*40*).

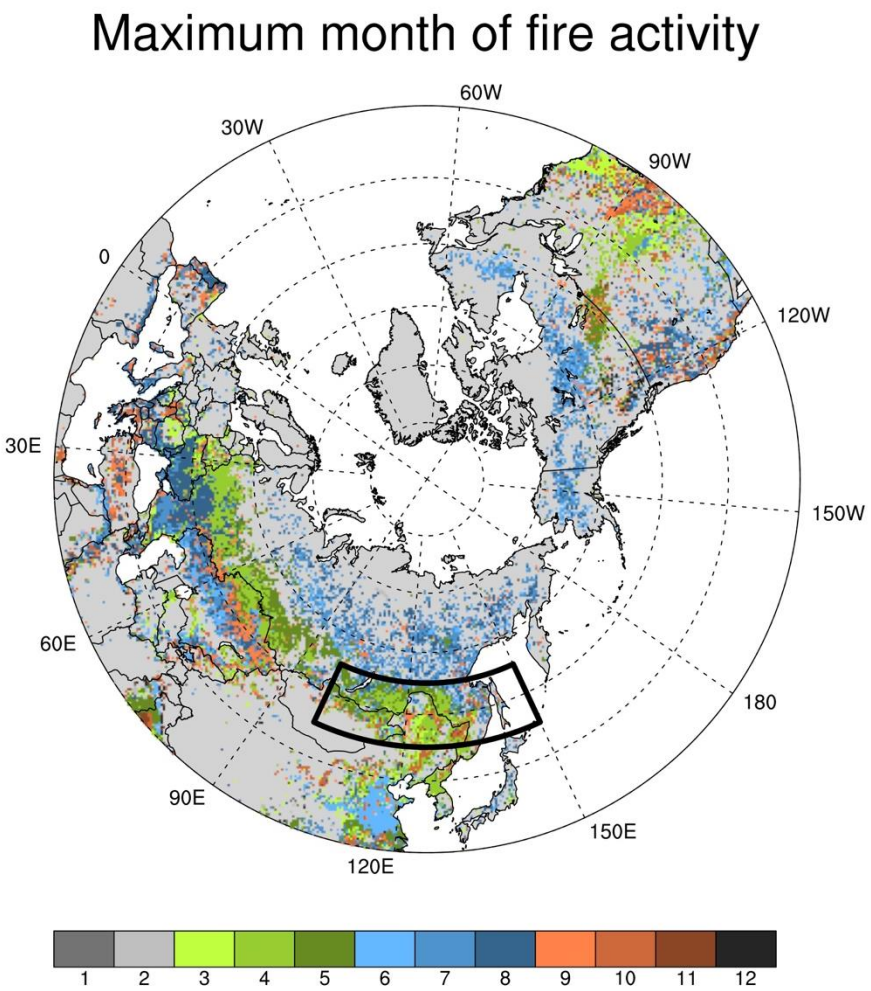

Fig. S1. Month of maximum of fire activity. The month of maximum burned area (January–December) displayed across the pan-Arctic region, which has more than 0.1% (fire return interval of 1000 years), based on the Global Fire Emissions Database version 4.1 with small fires (regridded to 0.5° × 0.5°).

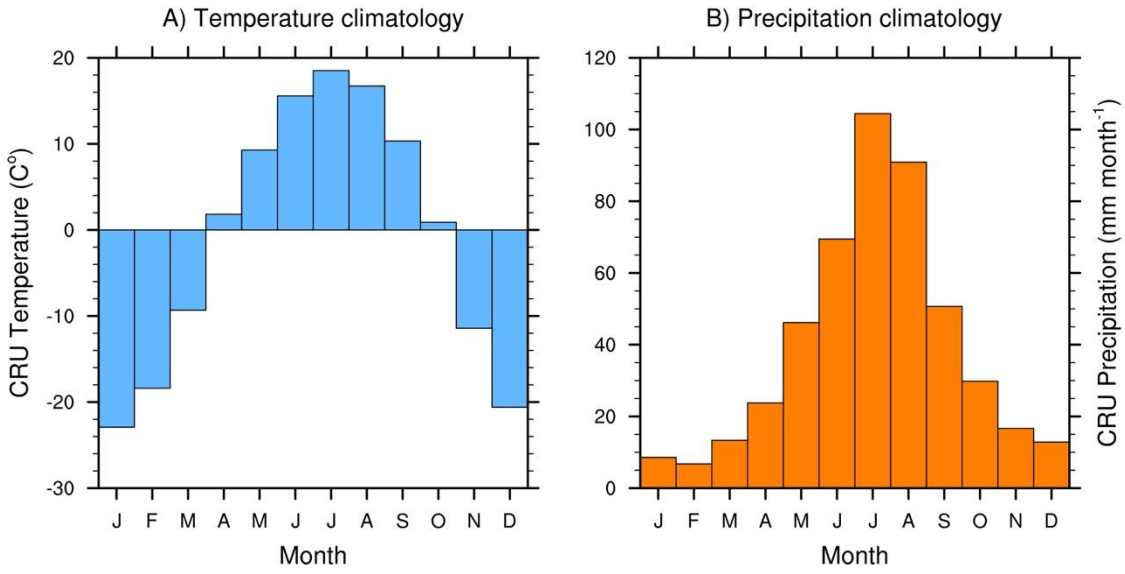

Fig. S2. Temperature and precipitation climatology. Monthly temperature (**A**) and precipitation climatology (**B**) over southeastern Siberia (100°–150°E, 45°–55°N) for 1997–2016.

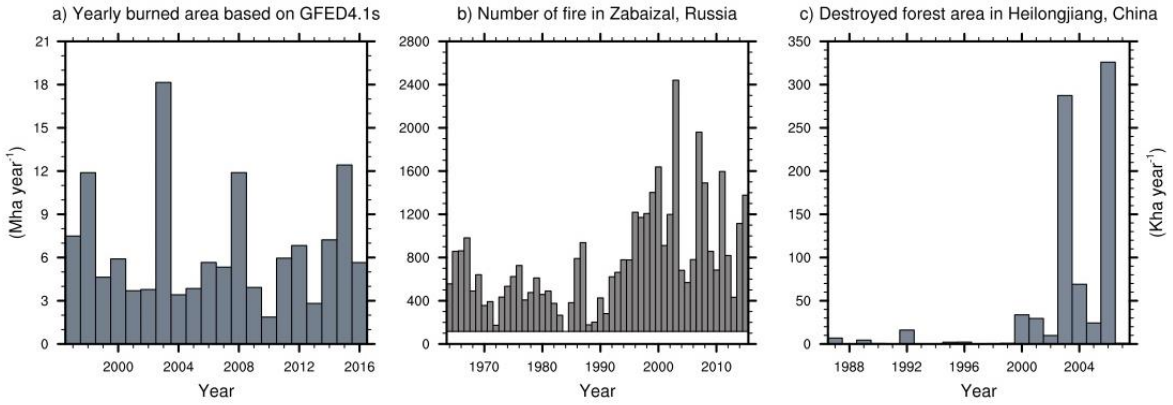

Fig. S3. Interannual variability of fire activity. (**A**) Yearly burned area over southeastern Siberia based on the Global Fire Emissions Database version 4.1 with small fires (GFED4.1s) for 1997–2016. (**B**) Number of fire observations in Zabaikal, Russia for 1964–2015 (http://лесслужба.забайкальскийкрай.рф). (**C**) Destroyed forest area in Heilongjiang, northeast China, for 1987–2007 (http://www.cfsdc.org).

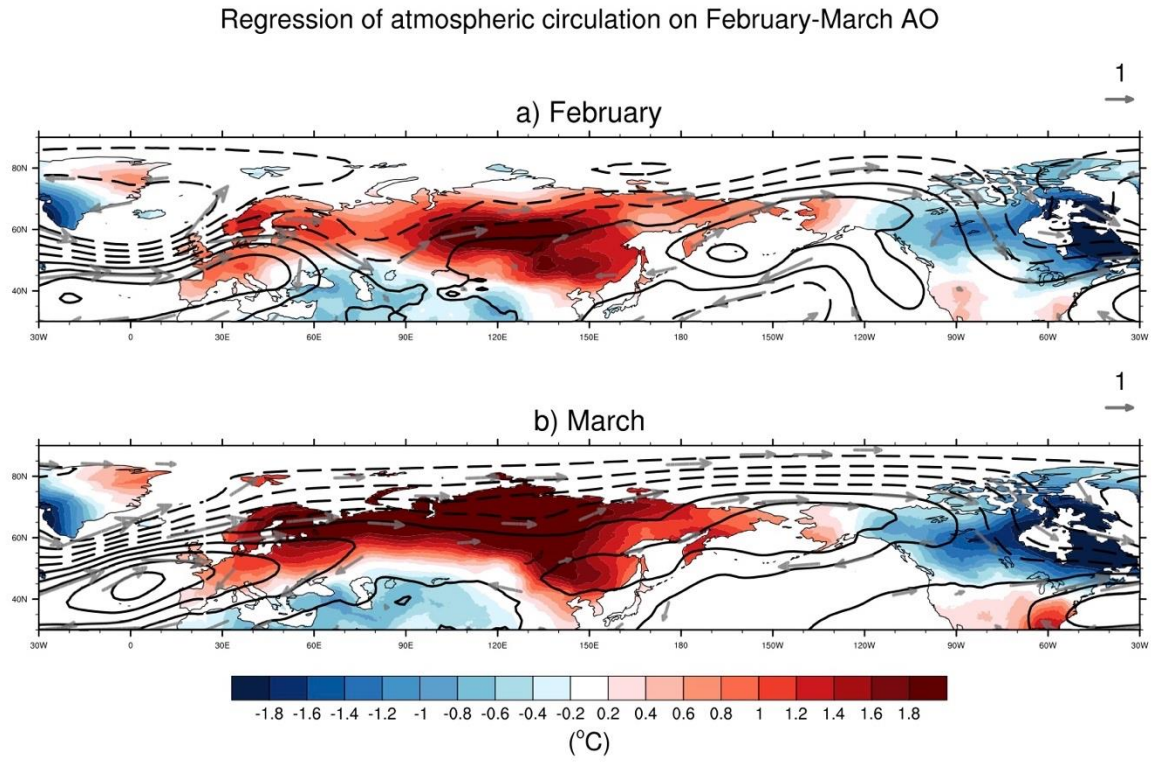

Fig. S4. Atmospheric circulation related to AO index. Regression coefficients of temperature (shading), 850-hPa geopotential height (contour; 100-gpm interval) and 850-hPa wind (vector) for February (**A**) and March (**B**) on February–March mean AO index. Wind vectors are displayed only in regions significant at the 95% confidence level based on a Student's *t*-test.

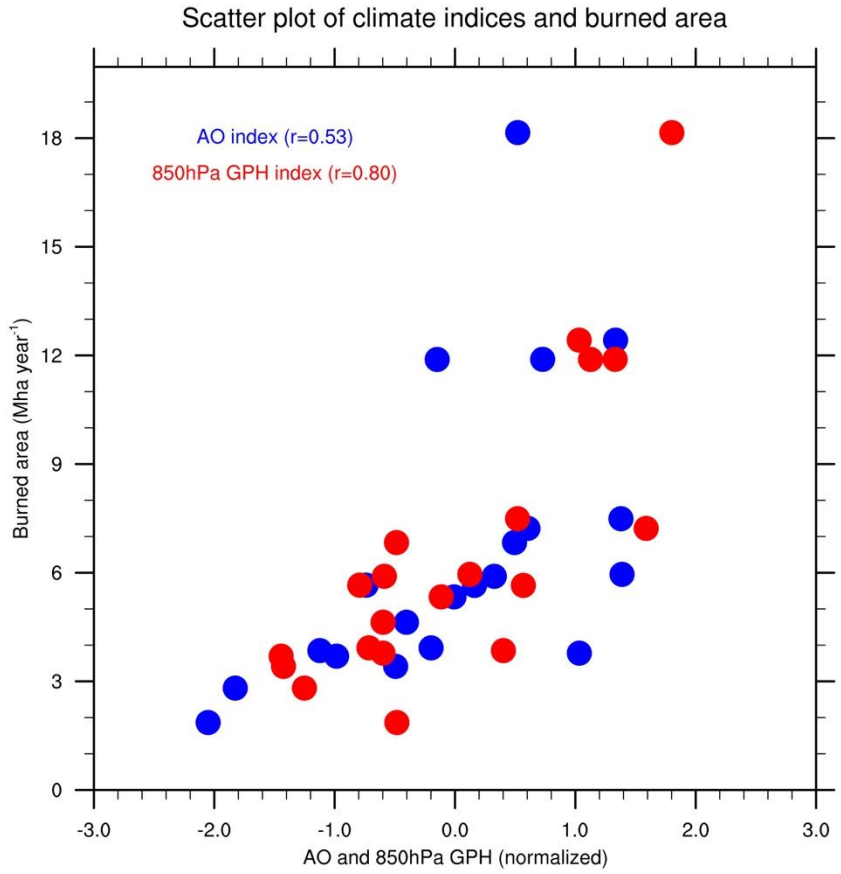

Fig. S5. Climate indices versus burned area over southeastern Siberia. Scatter plot of February–March mean AO index (blue) and 850-hPa geopotential height anomaly over southeastern Siberia (red) with yearly burned area (Mha year^{-1}) over southeastern Siberia.

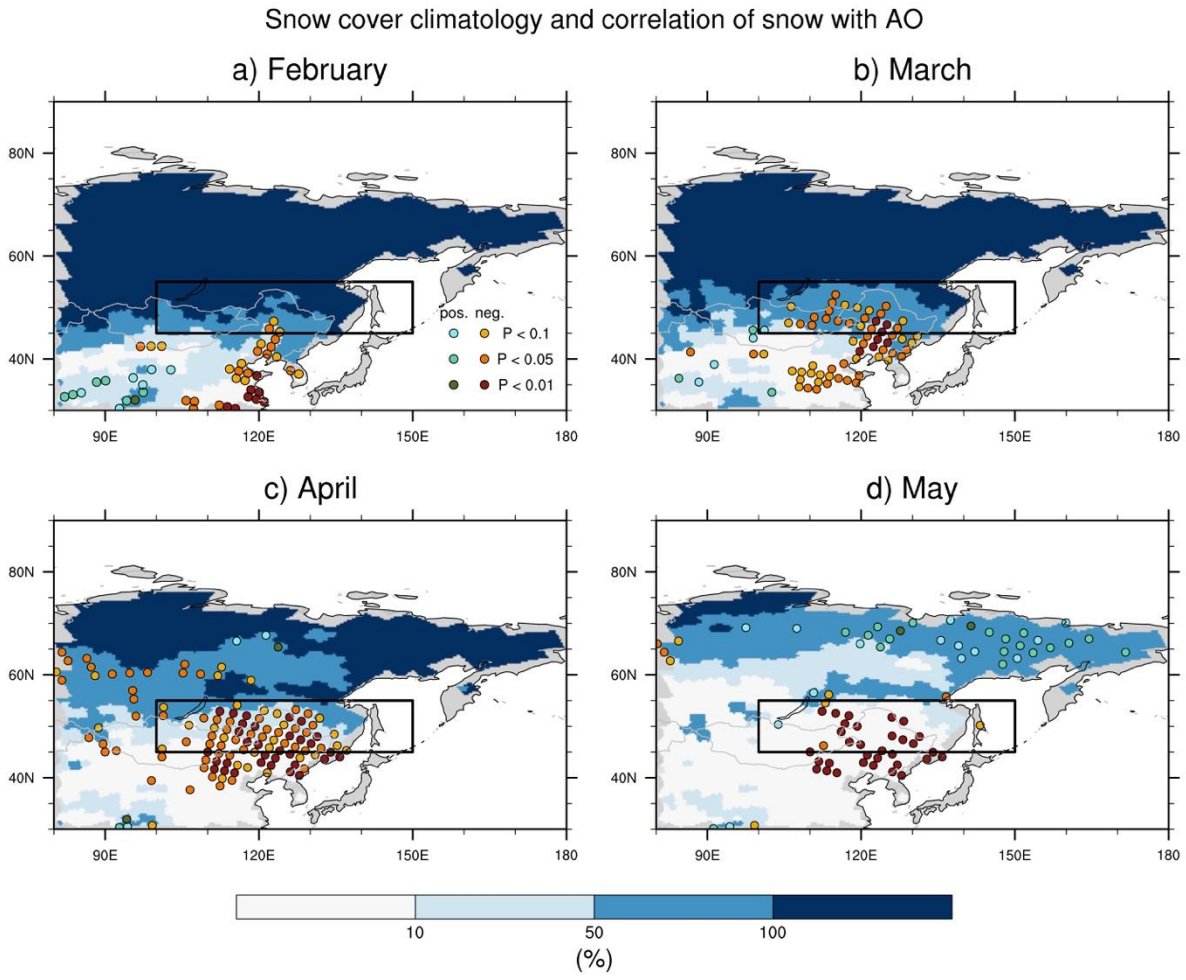

Fig. S6. Snow cover variation related to AO. Climatological monthly snow cover (shading) and statistical confidence (dots) based on correlation coefficient between February–March mean Arctic Oscillation index and monthly snow cover anomalies for February (**A**), March (**B**), April (**C**) and May (**D**) based on a Student's *t*-test.

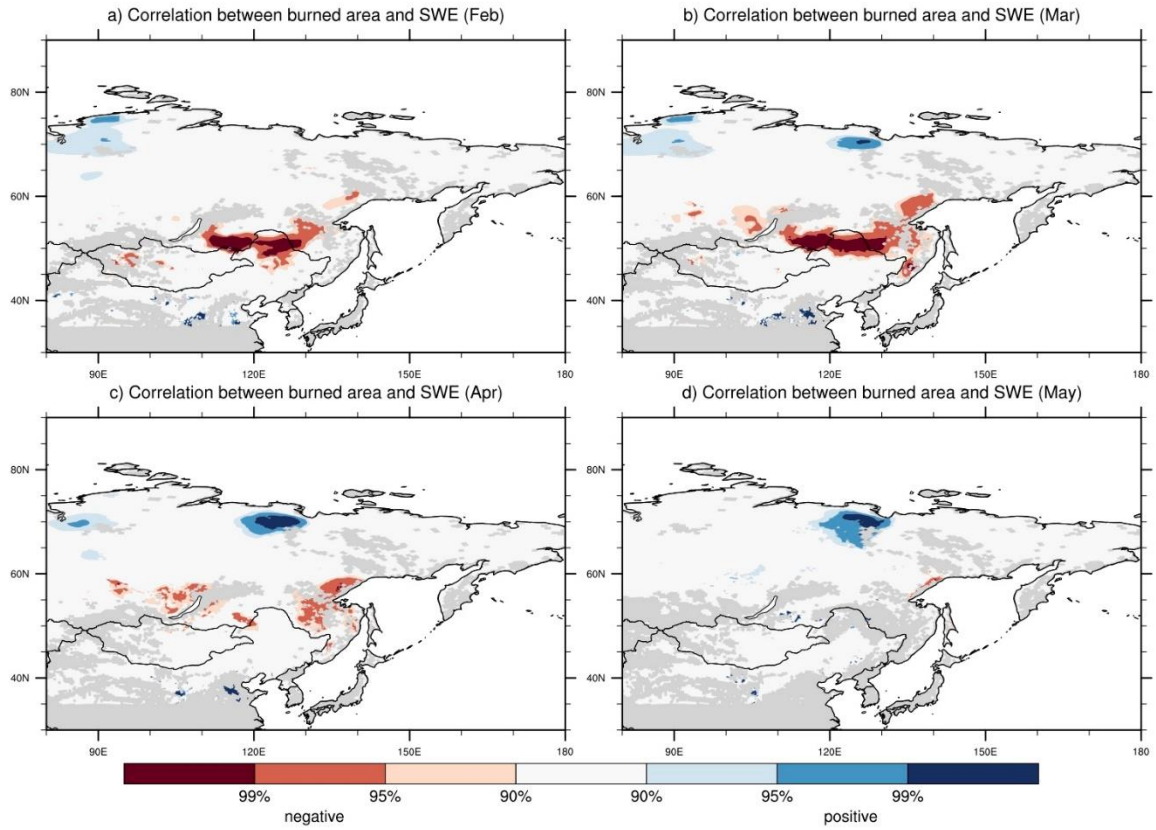

Fig. S7. Snow water equivalent variation related to fire activity over southeastern Siberia. Correlation significance map for yearly total burned area in southeastern Siberia and monthly snow water equivalent (*41*) (https://www.globsnow.info/swe/) anomalies for February (**A**), March (**B**), April (**C**) and May (**D**). Correlation significances displayed only in regions significant at the 90%, 95% and 99% confidence levels based on a Student's *t*-test.

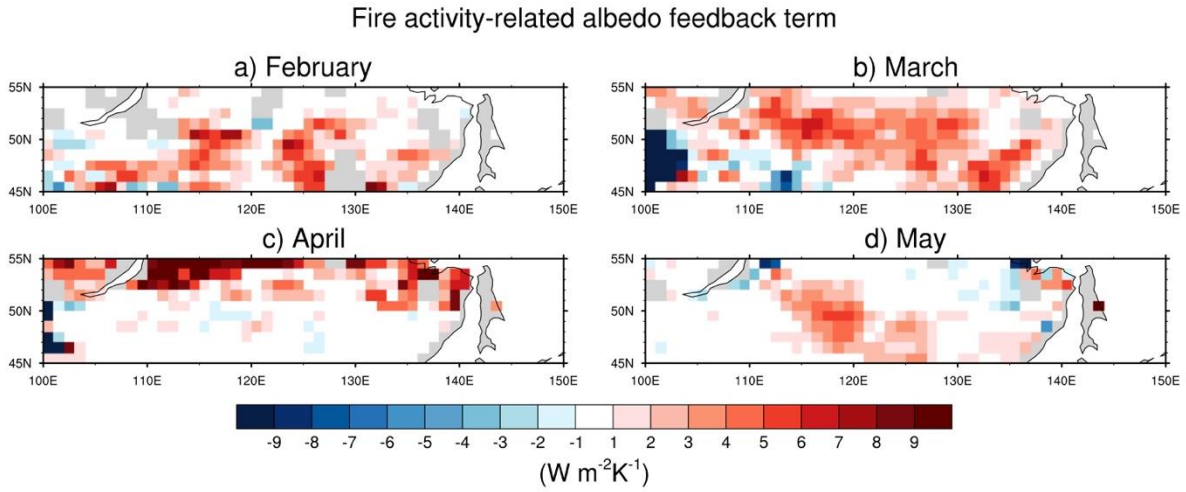

Fig. S8. Fire activity–related snow-albedo feedback term. Snow albedo feedback (W m^{-2} K^{-1}) can be quantified by the amount of additional net shortwave radiation at top of atmosphere as surface albedo decreases in association with a 1 °C temperature increase. Based on radiative kernel data, and regression coefficient of southeastern Siberian burned area on MODIS surface albedo and temperature anomalies, fire activity-related snow albedo feedback terms are quantified for February (**A**), March (**B**), April (**C**) and May (**D**). Radiative kernel data were obtained from Community Atmosphere Model version 3 (*42*) of National Center for Atmospheric Research (http://people.oregonstate.edu/~shellk/kernel.html).

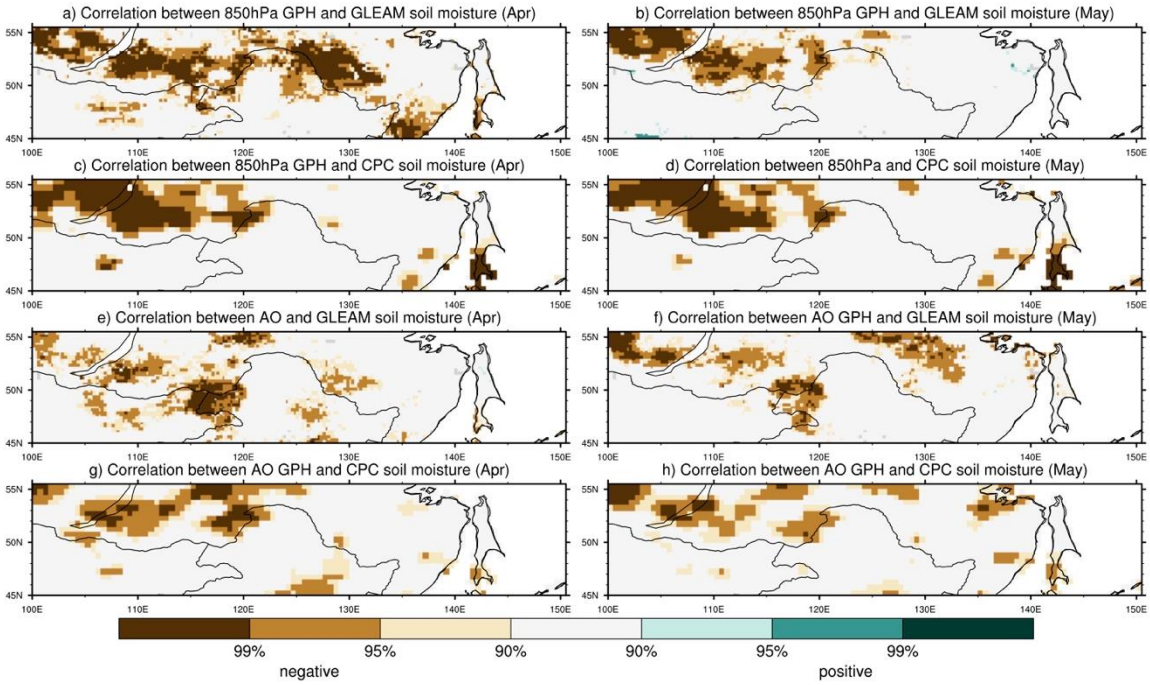

Fig. S9. Soil moisture anomalies related to 850-hPa geopotential height anomaly and AO index. Correlation significance map for February–March 850-hPa GPH/AO index and soil moisture anomalies in April (**A**, **C**, **E**, **G**) and May (**B**, **D**, **F**, **H**) based on Global Land Evaporation Amsterdam Model (GLEAM) (*43*) (https://www.gleam.eu) (A, B, C, D) and Climate Prediction Center (CPC) soil moisture data (*44*) (https://www.esrl.noaa.gov/psd/data/gridded/data.cpcsoil.html) (E, F, G, H) period 1997–2016. Correlation significances displayed only in regions significant at the 90%, 95% and 99% confidence levels based on a Student's *t*-test.

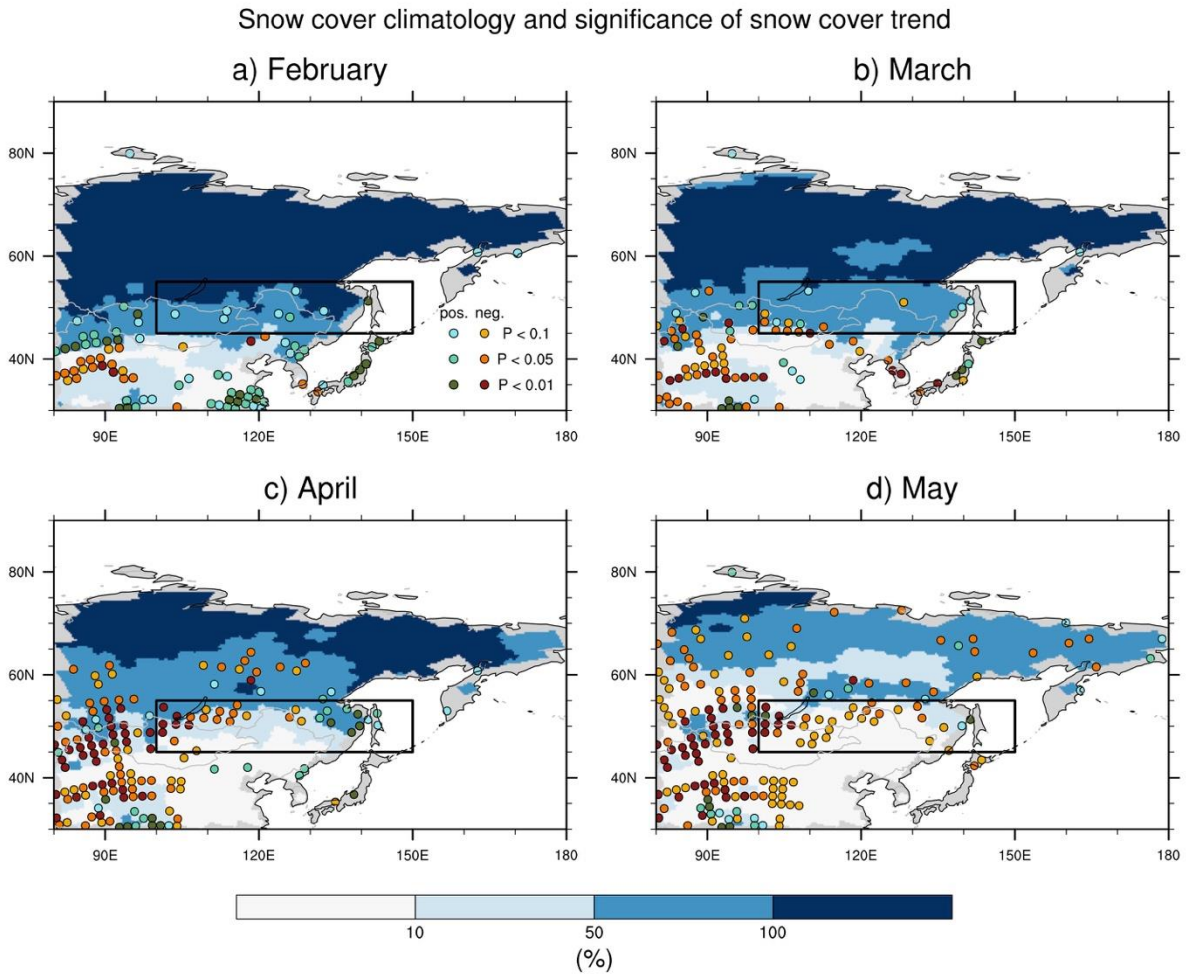

Fig. S10. Snow cover trend. Climatological snow cover (shading) and statistical confidence (dots) of snow cover trend for 1967–2016 for February (**A**), March (**B**), April (**C**) and May (**D**) based on a Student's *t*-test.